ORIGINAL PAPER

An ANN-Fuzzy Cognitive Map-Based Z-Number Theory to Predict Flyrock Induced by Blasting in Open-Pit Mines

Shahab Hosseini[1] · Rashed Poormirzaee[2] · Mohsen Hajihassani[3] · Roohollah Kalatehjari[4]

Abstract

Blasting is widely employed as an accepted mechanism for rock breakage in mining and civil activities. As an environmental side effect of blasting, flyrock should be investigated precisely in open-pit mining operations. This paper proposes a novel integration of artificial neural network and fuzzy cognitive map (FCM) with Z-number reliability information to predict flyrock distance in open-pit mine blasting. The developed model is called the artificial causality-weighted neural networks, based on reliability (ACWNNsR). The reliability information of Z-numbers is used to eliminate uncertainty in expert opinions required for the initial matrix of FCM, which is one of the main advantages of this method. FCM calculates weights of input neurons using the integration of nonlinear Hebbian and differential evolution algorithms. Burden, stemming, spacing, powder factor, and charge per delay are used as the input parameters, and flyrock distance is the output parameter. Four hundred sixteen recorded basting rounds are used from a real large-scale lead–zinc mine to design the architecture of the models. The performance of the proposed ACWNNsR model is compared with the Bayesian regularized neural network and multilayer perceptron neural network and is proven to result in more accurate prediction in estimating blast-induced flyrock distance. In addition, the results of a sensitivity analysis conducted on effective parameters determined the spacing as the most significant parameter in controlling flyrock distance. Based on the type of datasets used in this study, the presented model is recommended for flyrock distance prediction in surface mines where buildings are close to the blasting site.

Highlights

- An expert-based ANN is developed to predict blast-induced flyrock distance.
- A Fuzzy cognitive map and expert knowledge are used to simulate the weight of neurons.
- Z-number theory is employed to overcome the uncertainty of opinions.

✉ Roohollah Kalatehjari
r.kalatehjari@aut.ac.nz

Shahab Hosseini
h.seyyedshahab@modares.ac.ir

Rashed Poormirzaee
rashed.poormirzaee@gmail.com; r.poormirzaee@uut.ac.ir

Mohsen Hajihassani
m.hajihassani@urmia.ac.ir

[1] Faculty of Engineering, Tarbiat Modares University, Tehran, Iran

[2] Faculty of Environment, Urmia University of Technology, Urmia, Iran

[3] Faculty of Engineering, Urmia University, Urmia, Iran

[4] Built Environment Engineering Department, School of Future Environments, Auckland University of Technology, Auckland 1010, New Zealand

1 Introduction

Blasting is usually the first step in open-pit mining operation for rock breakage and is widely implemented in mining and civil projects. Although the primary goal of blasting is rock fragmentation, about 80% of the total energy of charged explosives is wasted in other ways. The wasted energy is dissipated in flyrock, air-overpressure (AOp), ground vibration, back break, and dust and fumes emission (Sari et al. 2014; Bakhtavar et al. 2021b; Zhou et al. 2020; Hosseini et al. 2021; Hajihassani et al. 2015; Khandelwal and Monjezi 2013a). Flyrock is determined as the rock fragments propelled beyond the blasting region by the energy of charges. The main reasons for flyrock production in blasting are an inappropriate design of the blasting pattern, inaccurate drilling work, inadequate stemming and burden, and unwarrantable specific charges (Yari et al. 2016). Blasting design parameters such as spacing, sub-drilling, powder factor, charge per delay, hole length, and stiffness factor are the most important controllable factors on flyrock distance (Khandelwal and Monjezi 2013b). On the other hand, rock mass characteristics such as rock density and rock mass rating (RMR) are the uncontrollable parameters in this process (Ghasemi et al. 2012a; b; Khandelwal and Monjezi 2013a, b; Rad et al. 2020).

Accurate flyrock prediction can prevent or minimize blasting-related fatal and nonfatal injuries (Ghasemi et al. 2012a; b). Recently, soft computing techniques have been used to predict flyrock distance in mining and civil engineering projects. The following paragraphs include a concise review of the recent application of different prediction methods with their success measured by R² values were available.

The least-squares support vector machines (LS-SVM) were used by Rad et al. (2018) to predict flyrock distance in the Gole-E-Gohar surface mine in Iran using data from 90 blastings. Their proposed model predicted the flyrock distance with an R^2 of 0.969. Kalaivaani et al. (2020) simulated the flyrock distance caused by bench blasting using an integrated recurrent fuzzy neural network (RFNN) with the Particle Swarm Optimization (PSO) algorithm. They used a dataset of 72 blastings and reached an R^2 of 0.933. Yari et al. (2016) predicted flyrock distance using a hybrid multilayer perception neural network (NN) and empirical models. They found the NN model more accurate than empirical models for flyrock distance prediction. An adaptive network-based fuzzy inference system (ANFIS) model was applied by Trivedi et al. (2015) and reported comparable results to the ANN and statistical models for flyrock prediction. In another study, Monjezi et al. (2012) successfully integrated multilayer perceptron NN (MLPNN) and genetic algorithm (GA) to predict blast-induced flyrock by a hybrid ANN-GA technique.

Faradonbeh et al. (2016) proposed genetic programming (GP) and gene expression programming (GEP) models to evaluate flyrock distance. They achieved R^2 values of 0.935 and 0.893 for their GP model's training and testing parts, respectively. Their GEP model achieved R^2 values of 0.991 and 0.987 for its training and testing, respectively, which suggested the GEP model was more accurate in predicting flyrock distance. Guo et al. (2021a) presented a combination of support vector regression models (SVRs) and Lasso and elastic-net regularized generalized linear model (GLM-NET) as the SVRs–GLMNET model to predict flyrock distance in a quarry mine. They developed six SVR models and imported training data into the GLMNET produced the most accurate results for flyrock distance prediction with an R^2 of 0.993.

In another recent attempt, Lu et al. (2020) develped an outlier robust ELM (ORELM) model for flyrock distance prediction and compared their results with extreme learning machine (ELM) and ANN models. They collected 82 blasting data by monitoring blasting events in 3 granite quarries for their study. Their ORELM model achieved an R^2 value of 0.958, providing higher accuracy than ANN with an R^2 value of 0.912 and ELM with an R^2 value of 0.955. In another research, Murlidhar et al. (2020) proposed an extreme learning machine (ELM) optimized by biogeography-based optimization (BBO) for flyrock distance prediction and used a particle swarm optimization (PSO)-ELM model for comparison. The R^2 values related to testing of PSO-ELM, BBO-ELM and ELM model were obtained as 0.93, 0.94, and 0.79, respectively, which proved the BBO-ELM a more reliable tool for flyrock distance estimation. In a study conducted by Guo et al. (2021b), the deep neural network (DNN) method was used to predict flyrock distance in Ulu Thiram quarry, Malaysia. They optimized the DNN model by whale optimization algorithm (WOA) and obtained the R^2 value of 0.9829 and 0.9781 for the training and testing dataset. Fattahi and Hasanipanah (2021) introduced an integrated model based on ANFIS and grasshopper optimization algorithm (GOA) to predict blast-induced flyrock in open-pit mines and obtained an R^2 value of 0.974. Hasanipanah et al. (2020a) proposed an adaptive dynamical harmony search (ADHS) algorithm to optimize the ANN architecture. They employed the ANN-ADHS to develop a model to estimate flyrock and predicted the flyrock distance with R^2 value of 0.929.

Researchers have also involved theoretical approaches and empirical models to predict the flyrock distance (Lundborg et al. 1975; Siskind and Kopp 1995; Raina et al. 2004; McKenzie 2009). Ghasemi et al. (2012b) proposed a theoretical approach for forecasting flyrock distance in a copper mine; Marto et al. (2014) developed a multivariate linear regression for flyrock prediction in surface mine; and in another study, an empirical model was presented for estimation of flyrock by Armaghani et al. (2016b).

In an attempt to integrate fuzzy systems with optimization techniques, Hasanipanah and Amnieh (2020) developed a fuzzy rock engineering system (FRES) for assessing the risk level of flyrock due to mine blasting. They successfully optimized their model using genetic algorithm (GA), imperialist competitive algorithm (ICA), and particle swarm optimization (PSO) and achieved the R^2 values of 0.984, 0.983, and 0.981, respectively. Bakhtavar et al. (2021a) used the fuzzy cognitive map (FCM) technique to analyze the relationship between dust emission parameters due to mine blasting. The FCM method with a fuzzy slack-based efficiency model was also used by Rezaee et al. (2021) to improve auto industry projects. The FCM framework has several primary advantages among other cognitive methods, including as (1) examining the causal-effect relationships between concepts (nodes) of the network, (2) reducing the complexity of decision-making problems, (3) decreasing dependence on experts' views and increasing the accuracy of the calculated weights by applying learning algorithms, and (4) reducing computational time (Bakhtavar et al. 2021a). Therefore, this research involves this method in predicting flyrock distance.

Zadeh (2011) first introduced the *Z*-number concept, which denotes a fuzzy number pair (*A*, *R*). This theory is a new concept in fuzzy logic that has been recently adopted in engineering applications. One of the advantages of *Z*-number theory is eliminating uncertainty in expert views (Hosseini et al. 2022; Poormirzaee and Hosseini 2021). Ghoushchi et al. (2019) applied reliability of *Z*-numbers for decreasing complexity of industries and risk assessment of processes. Aboutorab et al. (2018) employed the *Z*-evaluations to solve the uncertainty of supplier development problem. Stock selection problems were eliminated using *Z*-numbers by Yaakob and Gegov (2016). In another research, the *Z*-number theory was used by Tian et al. (2021) to manage uncertain information and for pattern recognition. Jiskani et al. (2022) used *Z*-number theory to overcome uncertation of expert views to analyze health and safety risks in surface mines. They integrated *Z*-numbers with fuzzy fualt tree analysis and concluded that this theory is capable of increasing the results accuracy. *Z*-number-based fuzzy system has been utilized in predicting food security risk levels by Abiyev et al. (2018). The uncertain environmental conditions in the supplier development problems was solved using an integrated *Z*-number theory with Best Worst Method proposed by Aboutorab et al. (2018). Yazdi et al. (2019) used *Z*-numbers for eliminating uncertainty of expert views in probabilistic risk assessment.

A novel soft computing-based model is presented in this research to predict flyrock distance in open-pit mining operations. This model is based on the integration of a multilayer perceptron neural network (MLPNN), fuzzy cognitive maps (FCMs), and *Z*-number theory. The proposed model is called the artificial causality-weighted neural networks based on reliability (ACWNNsR) and is the first study that simultaneously employs the ANN, FCM, and *Z*-numbers for flyrock prediction to the best of the authors' knowledge. The proposed model eliminates the uncertainties in the FCM modeling through the use of reliability information of *Z*-numbers. Notably, the weight of ANN neurons is simulated using the learned FCM by combining nonlinear Hebbian algorithm (NHL) and differential evolution (DE) algorithms, which is an improvement compared to previous models. Implementing the FCM based on *Z*-number in neurons weighting is expected to help predict the flyrock distance and provide a safer working environment for blasting operation.

2 Research Methodology

2.1 Artificial Neural Networks (ANNs)

Since the 1940s, ANNs have been first pioneered by McCulloch and Pitts (1943). They pointed that ANNs are capable of computing any logical or arithmetic function. The computations of neural signals human-brain inspire the concept of ANNs by translating them into a simple linear mathematical equation to establish an input–output relationship. Simulation of the learning process is one of the prominent characteristics of ANNs (Esmaeili et al. 2014). An original ANNs is structured based on three main components: learning rule, network training architecture, and activation function (Simpson 1990). The recurrent and back-propagation feed-forward neural networks are two major types of ANNs (Armaghani et al. 2015). Besides, the various architectures of ANNs such as radial basis function (RBF), multilayer perceptron neural networks (MLPNN), deep feed-forward neural networks (DFF), recurrent neural networks (RNN), extreme learning machine (ELM), echo state network (ESN), Bayesian regularized neural network (BRNN), generalized feed-forward neural networks (GFNN), etc. have been presented so far. However, optimal constructing of the ANN architecture is a challenge (Nguyen and Bui 2020; Hajihassani et al. 2015). Depending on the different applications of an ANN, various methods are presented to design an ANN.

2.2 Multilayer Perceptron Neural Network (MLPNN)

Multilayer perceptron neural networks (MLPNN) have been employed successfully to overcome different and complex engineering problems through supervised training using the error back-propagation algorithm. The feed-forward back-propagation neural network suggested by Shahin et al. (2002) is one of the most widely used ANNs in prediction aims (Armaghani et al. 2016a; Hoseinian et al. 2017; Alizadeh et al. 2021). An error-correction learning rule is

used in this algorithm, in which a backward and a forward pass are performed for error back-propagation learning to take place. In the forward pass, a learning process is initialized in nodes (input vector) of the networks, and conducted calculations propagate from the first layer to the last layer (Hosseini et al. 2021). Then, network outputs (actual response) are determined based on a set of inputs. In this process, the generated synaptic weights remain unchanged. However, the error-correction rule has been used to adjust the synaptic weights in the backward pass. In addition, an error signal is produced by subtracting network output from a desirable target. Synaptic connections are reversible as this error propagates backward (Esmaeili et al., 2014; Bakhtavar et al., 2021a).

A multilayer perception (MLP) is the famous and most well-known structure of ANN. This network is structured from three primary input, hidden, and output layers, each considering several neurons (nodes). As the simple form of a biological neuron, the nodes are connected to other nodes by an exclusive weight. The MLPNN receives the input data and propagates in a forward path. It should be noted that the weight value is initialized to make connections among input, hidden, and also output nodes, which are randomly assigned. The general architecture of an MLP is shown in Fig. 1.

MLP simulates the output value by Eq. (1):

$$y = f_i\left(\sum_{i=1}^{n} w_{ij}x_j + b_i\right), \tag{1}$$

where x and y indicate the input matrix and output value, respectively. w represents the weight vector, and b shows the bias value of each neuron. f indicates the activation (transfer) function. According to the various usage, the number of hidden layers and the number of hidden neurons in each hidden layer, learning algorithm, and activation function, can be different.

The created error during MLP training is calculated as follows:

$$e(w) = \frac{1}{n}\sum_{j=1}^{n}\sum_{i=1}^{I}(s_i - o_i), \tag{2}$$

where $e(w)$ is the MLP network error, w indicates tth iteration weight, s_i denotes output node, o_i represents output value of the ith output node, I signify output nodes number, and n stands patterns number. The main disadvantages of MLP are getting trapped in local minima and a slow learning rate. Researchers solve these difficulties by applying metaheuristic algorithms to optimize the weight of neurons and increase ANN performance (Taheri et al. 2017; Moosazadeh et al. 2019).
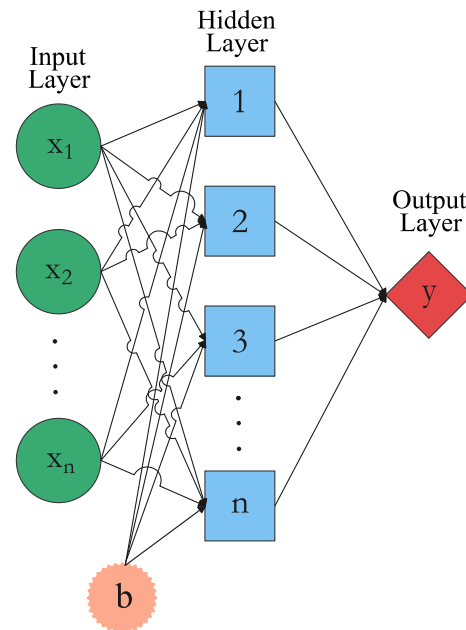

Fig. 1 General MLP architecture

2.3 Bayesian Regularized Neural Network (BRNN)

An ANN can be designed with various hidden nodes, so it is difficult to be determined precisely. Once overfitting occurs, the results will be unreliable if too many hidden neurons are considered. Inversely, an ANN with inadequate neurons has difficulty in the learning process. The Bayesian regularized neural network (BRNN) is proposed to overcome these problems by combining Bayes' theory into the regularization system. The learning process of the Bayesian scheme considers the uncertainty in the weight vector.

BRNN can be used for solving nonlinear problems effectively. BRNN was first basically presented by MacKay (1992), which focuses on the probabilistic learning operation of ANNs. The outstanding feature of BRNN is to determine the number of effective weights of the network. Based on this fact, an optimal network size is automatically determined based on the number of training cases needed for the learning process. BRNN, as one of the AI methods, employs the propagation algorithm which computes the amount of the least-squares error function as in Eq. (3) (Nguyen et al. 2020):

$$S(w) = \beta \sum_{i=1}^{n}(y_i - t_i)^2 + \alpha \sum_{i=1}^{m} w_i^2, \tag{3}$$

where α and β indicate the hyperparameters (regularization parameters). n indicates the number of data, w denotes the weight of inputs value, y signify the weight of output values, and t is the weight of target values.

BRNN performs best when the regularization parameters are set at their optimum. Based on a Bayesian model, the weights in the network can be operated as random elements. The weights are represented in the form of a density function, which is determined using Bayes' theorem (Kurnaz and Kaya, 2018):

$$P(w|\alpha, \beta, D) = \frac{P(D|w, \beta) \cdot P(w|\alpha)}{P(D|\alpha, \beta)}, \tag{4}$$

where $P(w|\alpha)$ denotes the prior density.

Before collecting databases, the degree to which the weights are known is signified by $P(w|\alpha)$. Furthermore, $P(D|w,\beta)$ indicates the possibilities function determined the probability of the error, and $P(D|\alpha,\beta)$ denotes model evidence or normalization parameter. Maximizing the posterior probability of the model can lead to optimal weights in the training process; thus, the error function of BRNN is obtained. Suppose the priority data and the probability distribution of weights be Gauss; weights are assigned a priority probability function with the following:

$$P(w|\alpha) = \frac{1}{Z_w(\alpha)} \cdot \left(e^{-\alpha E_w}\right). \tag{5}$$

The probability of errors, possibility, is formulated as:

$$P(D|w, \beta) = \frac{1}{Z_D(\beta)} \cdot \left(e^{-\beta E_w}\right). \tag{6}$$

The posterior distribution is achieved as Eq. (7):

$$P(w|\alpha, \beta, D) = \frac{1}{Z_S(\alpha, \beta)} \cdot \left(e^{-S(w)}\right). \tag{7}$$

The optimal Regularization parameters α, β are calculated through the Bayes theorem as follows:

$$P(\alpha, \beta|D) = \frac{P(D|\alpha, \beta) \cdot P(\alpha, \beta)}{P(D)}, \tag{8}$$

where $P(\alpha, \beta)$ and $P(D|\alpha, \beta)$ are the prior probabilities for the normalized parameters α, β, and the term of possibility, respectively. The optimum values of α, β are determined as Eqs. (9)–(11):

$$\alpha = \gamma/2E_w \tag{9}$$

$$\beta = (n - \gamma)/2E_D \tag{10}$$

$$\gamma = \sum_{i=1}^{m} m - \alpha \cdot \text{trace}^{-1}(A). \tag{11}$$

In which γ indicate the effective parameter, m is the number of parameters, and A denotes the objective function (Hessian matrix of $S(w)$).

2.4 Fuzzy Cognitive Maps (FCMs)

The cognitive map (CM) approach is widely employed in engineering since it can examine and obtain the complicated cause-and-effect interactions between several parameters (variables). Various parameters communicate complex relations with the other parameters supporting a cause-and-effect status in actual issues. A CM is structured to connect knots through organized arcs consisting of signs on the bow. In a precise scheme of a cognitive map, nodes denote unique theories which represent a system. In addition, arcs indicate cause-and-effect relations (weights) among the nodes.

The fuzzy CM (FCM) is a powerful method applied to specific problems in which the cost of collecting data is high or inaccessible. An FCM uses fuzzy numbers in the interval $[-1,1]$ or $[0,1]$ to explain intellectual opinion, which indicates the strength of attraction of causal relationships. The mental perspective of experts is crucial to design the map of FCM and predict concept weights and relationships between factors using neural network logic (Rezaee et al. 2017, 2018). A view of the cognitive map is presented in Fig. 2.

As illustrated in Fig. 2, C_i shows concepts (nodes) that are connected with weighted arcs. W_{ij} represents cause-and-effect relationships between C_i and C_j. $W_{ij} > 0$ and $W_{ij} < 0$ denote a positive and negative causal relationship, respectively. In addition, $W_{ij} = 0$ indicates no relationship among connected concepts.

It should be noted the weight of factors should not depend on expert opinions. However, the combination of Hebbian and metaheuristic algorithms is appropriate for adjusting map concept weights. This problem is solved by proposing learning algorithms that decrease dependency on expert views and simultaneously improve the weights and map convergence accuracy. Learning algorithms such as the Hebbian, hybrid, and population-based algorithms are used to apply the FCM (Papageorgiou and Kannappan 2012). This study integrates the nonlinear Hebbian algorithm (NHL) with the differential evolution (DE) algorithm to apply in FCM. The proposed hybrid algorithm is known as the NLH-DE algorithm, which can update non-dimensional weights in various simulations and maintain connections among nodes in a general map.

Different type of relationships between concepts shows the state vector $A = [A_1, A_2, …, A_n]$. The state vector A must continually transfer through the weight vector to develop a system. Hence, Eq. (12) is introduced to estimate the state vector A for each concept of C_i at repetition t:

Fig. 2 A view of the cognitive map
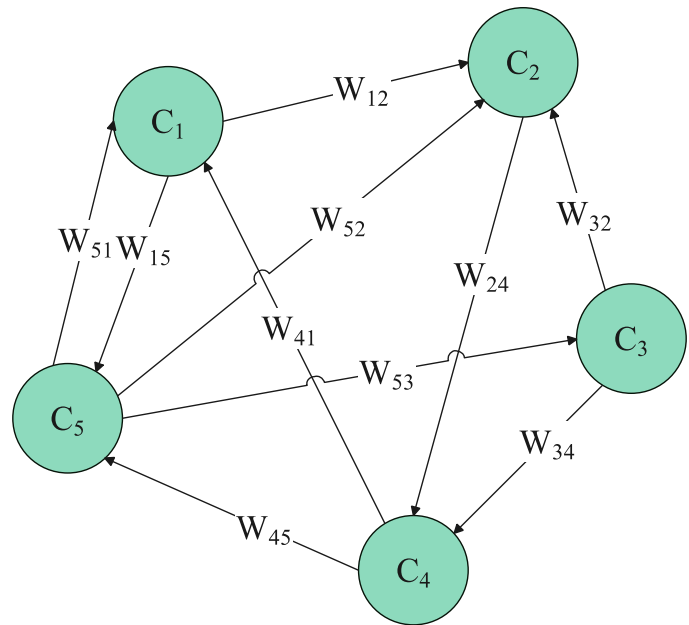
$$A_i^t = f\left(A_i^{t-1} + \sum_{\substack{j \neq i \\ j=1}}^{N} A_j^{t-1} \cdot W_{ij}\right), \qquad (12)$$

where A_t and A_{t-1} are the values of concept C_i at iteration t and $t-1$, respectively. W_{ij} denotes the connection weight through concept C_j to concept C_i. In addition, $f(x)$ indicates a threshold function. The unipolar sigmoid function (Eq. 13) is the best function to convert the result in the interval of [0, 1] or [−1, 1] compared among other threshold functions, where λ represents the function slope. State vector A is simulated using Eqs. (12) and (13), and the new value of A is updated, and this proceeds until convergence is achieved (Onari et al. 2020).

$$f(x) = \frac{1}{1 + e^{(-\lambda x)}}. \qquad (13)$$

2.5 *Z*-Number Concept

This theory was presented to overcome the numbers that are not reliable at all (Onari et al. 2020). Pair of Z-number (A, R) denotes restrictions to representing the behavior of the Z-numbers. Components of A and R describe a fuzzy set and degree of reliability, respectively. The degree of certainty can be denoted as a probability density function or a fuzzy set. For example, the production rate is announced as follows:

"daily blasted rocks in a large scale mine is about 1500 tons", low.

This announcement can be expressed as "X is $Z = (A, R)$." In contrast, X is the "daily blasted rocks" variable, A is a fuzzy set that expresses the daily blasted rocks "about 1500 tones", and R is the degree of certainty of A in the event that is "low" (Eq. 14).

$$R(X) = X \text{ is } A. \qquad (14)$$

Equation (14) describes probability constraint and A expressed probability distribution X. In this regard, it can be stated that:

$$R(X) : X \text{ is } A \rightarrow \text{Poss}(X = u) = \mu_A(u), \qquad (15)$$

where u is the general value of X and μ_A is the membership function of A, and set of A can be indicated as a restriction that is related to $R(X)$:

$$R(X) : X \text{ is } p, \qquad (16)$$

whereas p is the probability density function of X (Zadeh 2011):

$$R(X) : X \text{ is } p \rightarrow \text{Prob}(u \leq X \leq u + du) = p(u)du. \qquad (17)$$

The problem description by Z-numbers is clear; nevertheless, performing problem calculations by Z-numbers are comparatively difficult (Zadeh 2011). Z-numbers are disposed of accurately with their operations to overcome this problem, and transforming them into crisp numbers is investigated (Song et al. 2020). The complicated computational procedures of Z-number are solved by transforming Z-value to the fuzzy number or crisp value; however, this method significantly loses some information and decreases the advantages of using Z-information during information transformation (Onari et al.

Table 1 Expressed *Z*-numbers as linguistic values

Number	Linguistic terms	Membership function	
1	0% sure	(0, 0, 0.05)	Reliability (*R*)
2	5% sure	(0, 0.05, 0.1)	
3	10% sure	(0.05, 0.1, 0.15)	
4	15% sure	(0.1, 0.15, 0.2)	
5	20% sure	(0.15, 0.2, 0.25)	
6	25% sure	(0.2, 0.25, 0.3)	
7	30% sure	(0.25, 0.3, 0.35)	
8	35% sure	(0.3, 0.35, 0.4)	
9	40% sure	(0.35, 0.4, 0.45)	
10	45% sure	(0.4, 0.45, 0.5)	
11	50% sure	(0.45, 0.5, 0.55)	
12	55% sure	(0.5, 0.55, 0.6)	
13	60% sure	(0.55, 0.6, 0.65)	
14	65% sure	(0.6, 0.65, 0.7)	
15	70% sure	(0.65, 0.7, 0.75)	
16	75% sure	(0.7, 0.75, 0.8)	
17	80% sure	(0.75, 0.8, 0.85)	
18	85% sure	(0.8, 0.85, 0.9)	
19	90% sure	(0.85, 0.9, 0.95)	
20	95% sure	(0.9, 0.95, 1)	
21	100% sure	(0.95, 1, 1)	

2020). Therefore, triangular fuzzy numbers (TFNs) convert *Z*-number into fuzzy numbers. These conversion rules were first proposed for reliable linguistic variables. In this research, the first way is applied to *Z*-number conversion. The opinions of the team of experts require linguistic variables to explain each estimation (Table 1), which its membership function is illustrated in Fig. 3 schematically.

Figure 3 illustrates the reliability level of *Z*-number in the ranges 0–100%. The value of 100% is used for strong reliability, while 0% represents unreliability. In other words, experts used this scale to express their judgments confidence. Notably, the reliability level has hugely improved the obtained results; therefore, experts' judgments are modified based on reliability, and reliable results are presented.

Suppose $Z = (\tilde{A}, \tilde{R})$:

$$\{\tilde{A} = (x, u_{\tilde{A}}) | x \in [0, 1]\} \tag{18}$$

$$\{\tilde{R} = (x, u_{\tilde{R}}) | x \in [0, 1]\}. \tag{19}$$

The *Z*-numbers reliability is calculated as follows:

$$\alpha = \frac{\int x\mu_{\tilde{B}}(x)\ \mathrm{d}x}{\int \mu_{\tilde{B}}(x)\ \mathrm{d}x}. \tag{20}$$

Finally, crisp numbers of reliability are applied to the restriction:

$$\tilde{Z}^\alpha = \{(x, u_{\tilde{A}}) | u_{\tilde{A}^\alpha}(x) = \alpha u_{\tilde{A}}(x), x \in [0, 1]\}. \tag{21}$$

For example, Let a *Z*-number $Z = (\tilde{A}, \tilde{R})$ for the constraint. There is a linguistic variable 'High (*H*)' ($A = H$) with a reliability' 0.95% sure' ($R = 0.95\%$ sure). This is explained as follows:
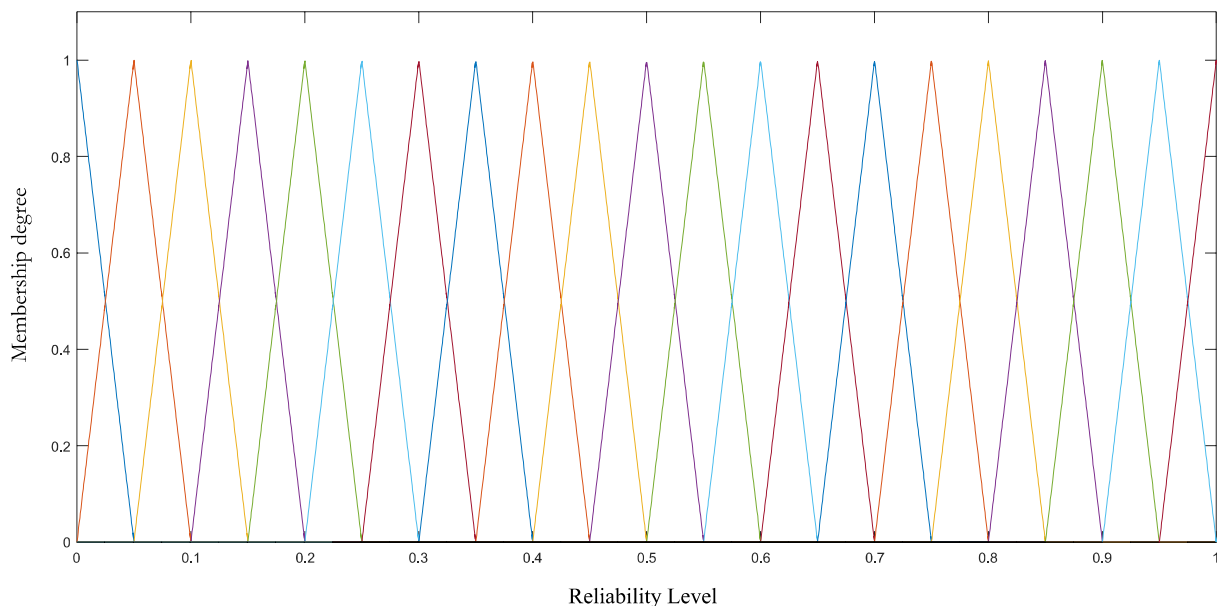
$$Z = [(5, 7, 9; 7), (0.9, 0.95, 1)].$$

Fig. 3 Linguistic term sets of *Z*-number

First, the reliability part is transformed to a crisp value as follows:

$$\alpha = \frac{\int x\mu_{\tilde{B}}(x)\,\mathrm{d}x}{\int \mu_{\tilde{B}}(x)\,\mathrm{d}x} = 0.95.$$

Second, the reliability weight is added to the restriction by:

$$\tilde{Z}^{\alpha} = (5, 7, 9; 0.95).$$

Finally, the weighted Z-number is changed into the regular fuzzy number.

$$\tilde{Z}' = (\sqrt{0.95} \times 5, \sqrt{0.95} \times 7, \sqrt{0.95} \times 9) = (4.87, 6.82, 8.77).$$

Figure 4 represented Z values after affecting the reliability, and the fuzzy number transformed from Z-number. Similarly, other Z-numbers are translated into TFNs.

2.6 Artificial Causality-Weighted Neural Networks Based on Reliability (ACWNNsR) Model

Figure 5 indicates the framework of the proposed ACWNNsR Model. As shown in the methodology framework, the effective parameters were first specified by literature investigations. Generally, the weight of each parameter is randomly calculated in the learning process of ANN. However, determining weights based on a learning rule is of particular importance. Therefore, the FCM technique simulated and updated parameter weights in different iterations. In addition, Z-number theory was applied to improve the expert's opinions in the matrix corresponding to causal-effect weights. Hence, the causal-effect weights were used in the ANN learning process. The results of the reliability FCM were finally utilized in the proposed ACWNNsR model. Finally, the sensitivity of flyrock to each input parameter was evaluated in two different methods.

3 Reference Case and Data Analysis

The required dataset for the study was collected from Anguran mine in Iran. This mine is one the large-scale and oldest lead–zinc mine in the Middle East, with an annual extraction rate of one million tons. According to Fig. 6, this mine is placed in Zanjan province at the west of Iran, at 47° 82′ 00″ E longitude and 36° 84′ 00″ N latitude, at an altitude of approximately 2935 m above sea level.

Figure 6 illustrates the location of the Anguran based on satellite imagery and a snapshot of blasting round. Blasting works are operated through 76, 114, and 127 mm blast holes. Blasting operations are principally conducted using ANFO (combine fuel oil and ammonium nitrate with a specific gravity of 0.85–0.95 g/cm^3). In this mine, flyrock distances were recorded from a total number of 416 blasting works. It should be noted that 416 blasting datasets were recorded during 4 years. Table 2 summarizes descriptive statistics of the collected data and their ranges. The frequency histogram of the flyrock distance is shown in Fig. 7. As shown in Fig. 7, 209 blasting events are accompanied by a flyrock distance of 100 m, while a flyrock distance of 340 m is observed in 7 blasting rounds. Notably, 204 blasting events caused 120 m long flyrock.

The B, St, S, Pf, MC, and flyrock factors measured in Anguran mine are variated in the range of 3–5 m, 0.9–0.8 m, 3–6 m, 0.01–1.67 kg/m3, 5.54–697.72 kg and 46.42–389.03 m, respectively. The parameters were immediately measured after performing the blasting pattern. This study defines the flyrock as the maximum distance to which rocks are impelled outside the blast location. Due to the difficulty in measurement of flyrock distance, part of the bench was painted before operating each blast rounds, and blasting was recorded on video. The maximum distance related to fragment rocks was measured using tracking fragment rocks. Note that the Pf and CD were calculated using other measured parameters.

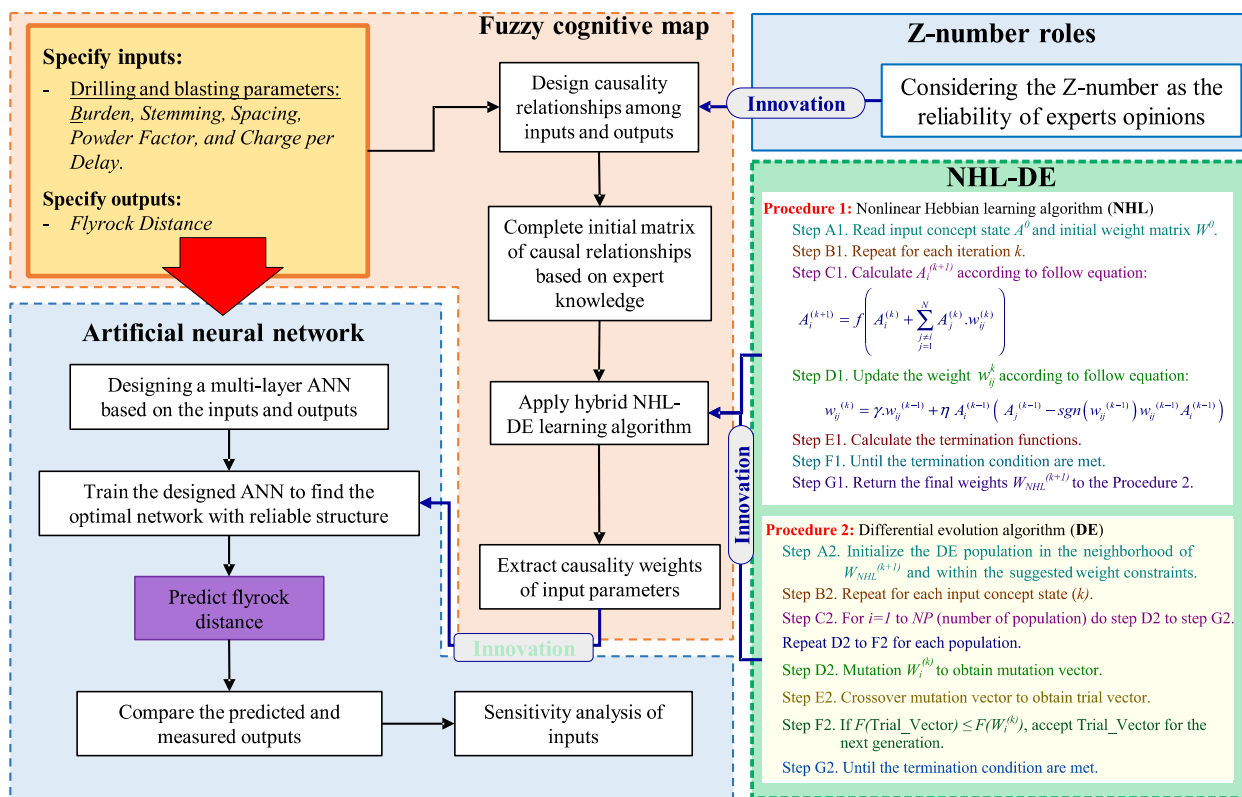**Fig. 4** Converting of Z-number to fuzzy number
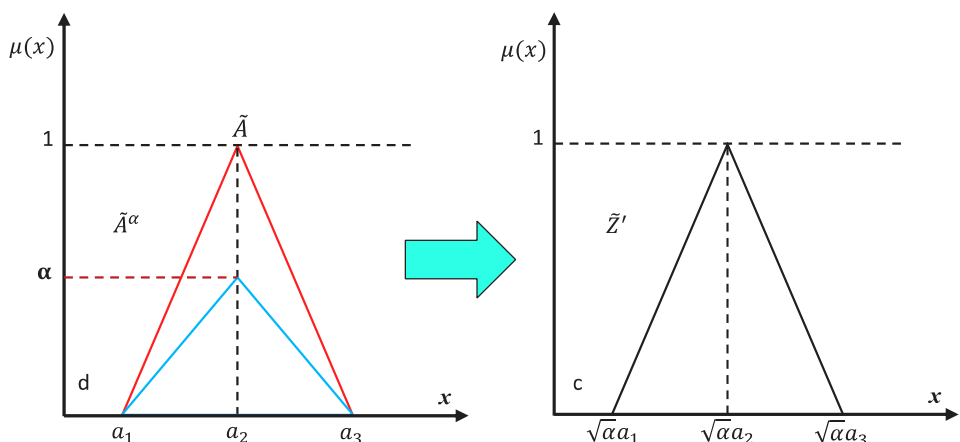
Fig. 5 The framework of the proposed ACWNNsR model

4 Flyrock Prediction

In this research, MLPNN, BRNN, and the proposed ACWNNsR models were employed to predict the flyrock distance due to mine blasting. First, 416 collected datasets were randomly divided into two main parts; training and testing datasets. Subsequently, the normalized values of inputs and outputs variables were calculated using the following equation:

$$x_n = \frac{x_i - x_{\min}}{x_{\max} - x_{\min}}. \tag{22}$$

In which x_n is the normalized value, x_i indicates the measured data, and $x_{\min}$, and $x_{\max}$ are the minimum and maximum values of data, respectively. The performance of the proposed models was evaluated employing three statistical criteria, including coefficient of determination (R^2), root-mean-squared error (RMSE), and value account for (VAF) (Keshtegar et al. 2021; Hasanipanah et al. 2020b), which are determined as follows:

$$R^2 = 1 - \left(\frac{\sum_{i=1}^{n} (O_i - P_i)^2}{\sum_{i=1}^{n} (P_i - \overline{P}_i)^2} \right) \tag{23}$$

$$\text{RMSE} = \sqrt{\frac{1}{n} \sum_{i=1}^{n} (O_i - P_i)^2} \tag{24}$$

$$\text{VAF} = 100 \cdot \left(1 - \frac{\text{var}(O_i - P_i)}{\text{var}(O_i)} \right), \tag{25}$$

where O_i and P_i are measured and predicted amounts, respectively; $\overline{P}_i$ is the average of the predicted values, and n is the number of datasets.

4.1 Prediction of Flyrock by MLPNN

In this study, MLP neural network is employed to flyrock prediction Anguran lead–zinc mine. In this regard, five effective parameters and flyrock are considered inputs and outputs of the modeling process. The maximum number of the hidden layer(s) is considered two layers, and the number of hidden nodes is determined based on the trial-and-error procedure. The MLP architectures are structured based on 3–23 hidden nodes; 100 training epochs are fixed. The statistical indicators formulated in Eqs. (23) to (25) are calculated for each trained structure. Then the best optimal architecture with high performance

Fig. 6 The geographical location of Anguran mine and blasting rounds

Table 2 Descriptive statistics of the recorded blasting parameters

Parameter	Sign	Unit	Min	Max	Mean	Std
Inputs						
Burden	B	m	3.00	5.00	4.08	0.29
Stemming	St	m	0.90	8.00	3.41	0.77
Spacing	S	m	3.00	6.00	4.93	0.30
Powder factor	Pf	kg/m^3	0.01	1.67	0.34	0.12
Charge per delay	CD	kg	5.54	697.72	173.76	69.92
Output						
Flyrock	Fr	m	46	389	124.27	44.25

Fig. 7 Frequency distributions of the flyrock distances
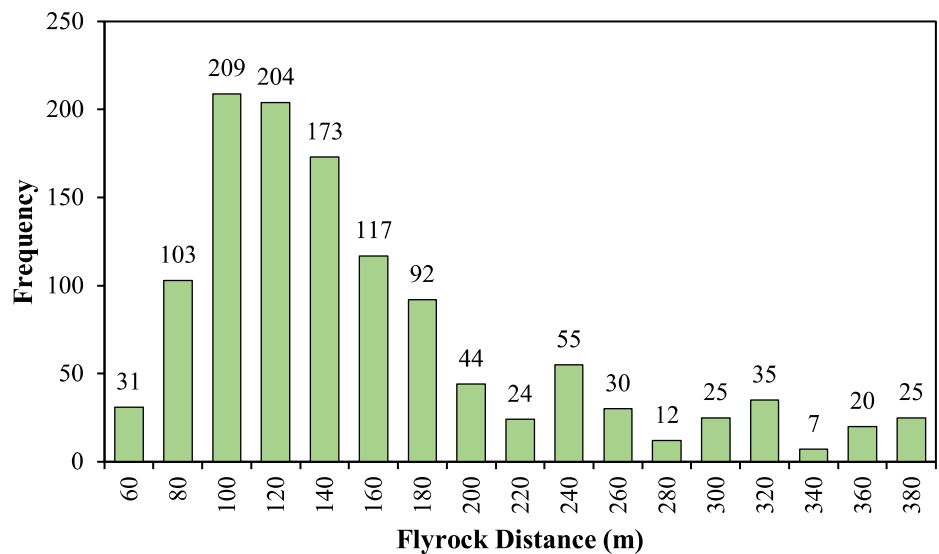
on both test and train phase is selected using the scoring system presented by Zorlu (Zorlu et al. 2008). In this technique, a score is assigned for each training and testing dataset and the highest score is considered to be the best model. The MLP modeling with different numbers of the hidden layer(s) and node(s) along with the rating of indices are presented in Table 3. As a result, the MLP4 with a total rate of 57 from 60 predicts the flyrock better than other architecture. Therefore, the best model with the optimal structure is the MLP4 model with a 5-10-1 structure.

4.2 Prediction of Flyrock by BRNN

In this section, the flyrock distance is predicted using BRNN predictive model. The number of hidden nodes causes complexity in the BRNN modeling process. Therefore, stopping criteria is determined based on the number of hidden neurons. A range between 1 and 8 was considered for the number of hidden neurons to prevent overfitting and learning

problems. Several trained BRNN models were achieved using the trial–error procedure and evaluated using performance indices to select the best BRNN structure capable of predicting flyrock distance with a high degree of accuracy.

The obtained results from BRNN modeling are tabulated in Table 4. The best model is selected by Zorlu scoring system. As it can be seen, BRNN, with the total rate value of 45 from 48, attained the highest value among eight architectures. Hence, it was concluded that the BRNN with a 5-5-1 structure is the best to predict blast-induced flyrock in the reference case.

4.3 Prediction of Flyrock by ACWNNsR

A learned FCM based on the NHL and DE hybrid learning algorithm was developed to calculate the weight linked to the hidden layers of ANN. In this regard, the cause-and-effect relationships between concepts (effective parameters and flyrock distance) were initialized using an expert

Table 3 Obtained performance indices to detect the optimum MLPNN model

Model	MLP architecture	Train			Test			Train rating			Test rating			Toral rate	Total rank
		R^2	RMSE	VAF	R^2	RMSE	VAF	R^2	RMSE	VAF	R^2	RMSE	VAF		
MLP 1	5-3-1	0.891	6.421	89.061	0.839	6.079	83.900	3	7	3	2	10	1	26	9
MLP 2	5-5-1	0.892	6.259	89.195	0.876	7.197	87.469	4	8	4	4	5	5	30	6
MLP 3	5-7-1	0.888	6.489	88.800	0.886	6.308	88.641	2	6	2	6	9	7	32	5
MLP 4	5-10-1	0.932	5.000	93.849	0.909	6.618	92.188	10	9	10	10	8	10	57	1
MLP 5	5-3-5-1	0.907	7.616	90.658	0.873	7.897	87.298	8	5	8	3	2	3	29	8
MLP 6	5-5-7-1	0.930	4.869	93.020	0.883	8.819	84.002	9	10	9	5	1	2	36	3
MLP 7	5-7-9-1	0.885	7.881	88.537	0.803	6.803	87.807	1	1	1	1	7	6	17	10
MLP 8	5-8-10-1	0.894	7.818	89.421	0.902	7.056	87.336	5	2	5	8	6	4	30	6
MLP 9	5-9-12-1	0.898	7.771	89.834	0.909	7.287	90.260	6	4	6	9	4	9	38	2
MLP 10	5-10-13-1	0.900	7.814	90.050	0.891	7.896	89.112	7	3	7	7	3	8	35	4

Table 4 Obtained performance indices to detect the optimum BRNN model

Model	BRNN architecture	Train			Test			Train rating			Test rating			Total rate	Total rank
		R^2	RMSE	VAF	R^2	RMSE	VAF	R^2	RMSE	VAF	R^2	RMSE	VAF		
BRNN 1	5-1-1	0.903	7.890	90.296	0.883	6.738	87.838	1	1	1	3	4	3	13	7
BRNN 2	5-2-1	0.932	4.954	93.242	0.912	5.606	91.195	4	4	4	7	7	6	32	4
BRNN 3	5-3-1	0.917	7.605	92.653	0.908	6.781	94.676	3	3	3	6	3	8	26	5
BRNN 4	5-4-1	0.912	7.744	91.203	0.770	7.407	71.755	2	2	2	1	2	2	11	8
BRNN 5	5-5-1	0.949	4.605	94.226	0.921	4.350	92.267	8	8	8	8	8	7	47	1
BRNN 6	5-6-1	0.933	4.757	93.562	0.848	13.499	59.238	5	7	5	2	1	1	21	6
BRNN 7	5-7-1	0.938	4.903	93.825	0.901	5.647	89.489	7	5	7	4	6	4	33	2
BRNN 8	5-8-1	0.936	4.851	93.613	0.902	6.251	89.587	6	6	6	5	5	5	33	2

team's opinion. It should be noted that experts expressed their opinions at all stages by applying the Z-number reliability in the interval 0–100%. An example of expert opinions and the reliability of opinions are tabulated in Table 5. The effect of Z value in their opinions is tabulated in Table 6.

The final matrix resulting from integrating an expert team of six-member opinions is reported in Table 7, which indicates the cause-and-effect relationships between the inputs and output variables.

This obtained matrix is used in the proposed FCM method as an initial matrix. Subsequently, an initial matrix was trained by applying hybrid NHL-DE algorithms to reduce the expert opinion and weighting errors dependency. Dynamic FCM solved this matrix and resulted in concept

weight as a final point. The weighting outcomes by the proposed FCM model based on the hybrid NHL-DE algorithms are shown in Fig. 8.

The weighting effective parameters using the proposed FCM provides more realistic results than the weighting method based on random numbers in a usual ANN. As illustrated in Fig. 8, the trained FCM shows weights among intervals [0, 1] and the sensitivity level of each parameter on the target node, which can be interpreted. According to the concept of cause-and-effect, burden and charge per delay with weights of 0.707 and 0.648 denote the highest sensitivity and effect weights on fly-rock distance.

The weightings of effective parameters are imported into an ANN architecture. Figure 9 shows the employed

Table 5 Example of expert opinion

	(A, R)	B	St	S	Pf	Cd	FR
B	Constraint	(0, 0, 0)	(0.5, 0.7, 0.9)	(0.3, 0.5, 0.7)	(0.7, 0.9, 1)	(0, 0, 0)	(0, 0, 0)
	Reliability (α)	(0, 0, 0)	(0.7, 0.75, 0.8)	(0.75, 0.8, 0.85)	(0.8, 0.85, 0.9)	(0.75, 0.8, 0.85)	(0, 0, 0)
		0	0.866	0.894	0.922	0.894	0
St	Constraint	(0, 0, 0)	(0, 0, 0)	(0.3, 0.5, 0.7)	(0.3, 0.5, 0.7)	(0, 0, 0)	(0, 0, 0)
	Reliability (α)	(0.75, 0.8, 0.85)	(0, 0, 0)	(0.5, 0.55, 0.6)	(0.6, 0.65, 0.7)	(0.7, 0.75, 0.8)	(0, 0, 0)
		0.894	0	0.742	0.806	0.866	0
S	Constraint	(0, 0, 0)	(0.3, 0.5, 0.7)	(0, 0, 0)	(0, 0, 0)	(0, 0, 0)	(0, 0, 0)
	Reliability (α)	(0.8, 0.85, 0.9)	(0.4, 0.45, 0.5)	(0, 0, 0)	(0.55, 0.6, 0.65)	(0.7, 0.75, 0.8)	(0, 0, 0)
		0.922	0.671	0	0.775	0.866	0
Pf	Constraint	(0, 0, 0)	(0.3, 0.5, 0.7)	(0.7, 0.9, 1)	(0, 0, 0)	(0.5, 0.7, 0.9)	(0, 0, 0)
	Reliability (α)	(0.6, 0.65, 0.7)	(0.6, 0.65, 0.7)	(0.9, 0.95, 1)	(0, 0, 0)	(0.6, 0.65, 0.7)	(0, 0, 0)
		0.806	0.806	0.975	0	0.806	0
Cd	Constraint	(0, 0, 0)	(0.3, 0.5, 0.7)	(0.5, 0.7, 0.9)	(0.5, 0.7, 0.9)	(0, 0, 0)	(0, 0, 0)
	Reliability (α)	(0.85, 0.9, 0.95)	(0.75, 0.8, 0.85)	(0.8, 0.85, 0.9)	(0.85, 0.9, 0.95)	(0, 0, 0)	(0, 0, 0)
		0.949	0.894	0.922	0.949	0	0
FR	Constraint	(0.3, 0.5, 0.7)	(0.3, 0.5, 0.7)	(0.7, 0.9, 1)	(0.7, 0.9, 1)	(0.5, 0.7, 0.9)	(0, 0, 0)
	Reliability (α)	(0.7, 0.75, 0.8)	(0.7, 0.75, 0.8)	(0.9, 0.95, 1)	(0.75, 0.8, 0.85)	(0.85, 0.9, 0.95)	(0, 0, 0)
		0.866	0.866	0.975	0.894	0.949	0

Table 6 Final value of one of the expert opinions

	B	St	*S*	Pf	Cd	FR
B	(0, 0, 0)	(0.433, 0.606, 0.779)	(0.268, 0.447, 0.626)	(0.645, 0.83, 0.922)	(0, 0, 0)	(0, 0, 0)
St	(0, 0, 0)	(0, 0, 0)	(0.222, 0.371, 0.519)	(0.242, 0.403, 0.564)	(0, 0, 0)	(0, 0, 0)
S	(0, 0, 0)	(0.201, 0.335, 0.47)	(0, 0, 0)	(0, 0, 0)	(0, 0, 0)	(0, 0, 0)
Pf	(0, 0, 0)	(0.242, 0.403, 0.564)	(0.682, 0.877, 0.975)	(0, 0, 0)	(0.403, 0.564, 0.726)	(0, 0, 0)
Cd	(0, 0, 0)	(0.268, 0.447, 0.626)	(0.461, 0.645, 0.83)	(0.474, 0.664, 0.854)	(0, 0, 0)	(0, 0, 0)
FR	(0.606, 0.649, 0.696)	(0.260, 0.433, 0.606)	(0.682, 0.877, 0.975)	(0.626, 0.805, 0.894)	(0.474, 0.664, 0.854)	(0, 0, 0)

Table 7 The causal-and-effect relationship between inputs and output variables

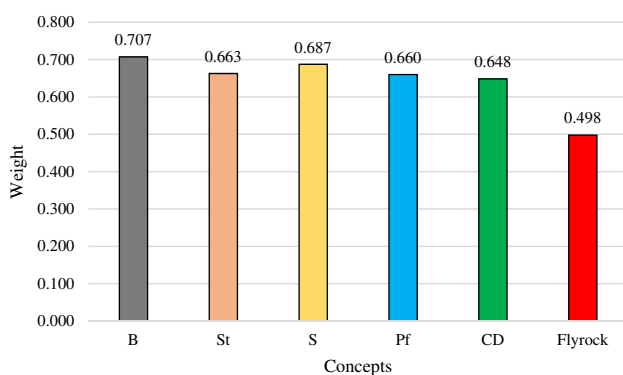|	*B*	St	*S*	Pf	Cd	FR
B	0	0.47	0.23	0.21	0.29	-0.73
St	0.17	0	0.26	0.41	-0.13	-0.59
S	0.37	-0.19	0	-0.17	-0.38	-0.48
Pf	0.61	-0.36	0.28	0	0.53	0.38
Cd	0.42	0.1	0.28	0.23	0	0.47
FR	0	0	0	0	0	0

weights in the MLP process. Ten trained ACWNNsR

Fig. 8 Weighting outcomes by the proposed FCM model

models were achieved by means of the trial-and-error method and evaluated using R^2, RMSE, and VAF, to select the best architecture. The obtained results are reported in Table 8. The ACWNNsR7 is the best structure that can be used to predict flyrock distance accurately.

5 Result and Discussion

The current paper developed the MLP, BRNN, and ACWNNsR models to estimate flyrock distance in surface mines. The comparative analyses related to calculating statistical indices (R^2, RMSE, and VAF) are tabulated in Table 9. The results show that the ACWNNsR model (with R^2 (0.996, 0.991), RMSE (1.404, 2.535), and VAF (99.867, 99.136)) performed better in estimating blast-induced flyrock distance compared to the BRNN model with R^2 (0.949, 0.921), RMSE (4.605, 4.350), and VAF (94.226, 92.267) and also MLP model with R^2 (0.932, 0.909), RMSE (5.000, 6.618), and VAF (93.849, 92.188). Furthermore, measured flyrock compared to predicted values by MLP, BRNN, and ACWNNsR models for 416 blasting rounds is plotted in Figs. 10, 11, 12, respectively. The correlation of the ACWNNsR model shows a significant relationship between the actual and estimated flyrock. Figure 13 shows the error in flyrock distance predicted by the ACWNNsR, BRNN, and MLP models for all 83 blasting events (testing dataset), comparing them with the recorded flyrock. These results show that the ACWNNsR model can predict the flyrock diatance more accurately than the MLP and BRNN models in training and testing datasets.

6 Sensitivity Analysis

The effectiveness and relative significance of the controllable parameters burden (*B*), stemming (St), spacing (*S*), powder factor (Pf), and charge per delay (CD) on the flyrock distance was evaluated using a sensitivity analysis. The cosine amplitude method (CAM) (Jong and Lee 2004) and partial derivatives (PaD) method (Gevrey et al. 2003) were used in this sensitivity analysis as shown in Eqs. (26) and (27). The sensitivity analysis results are shown in Fig. 14, which shows the
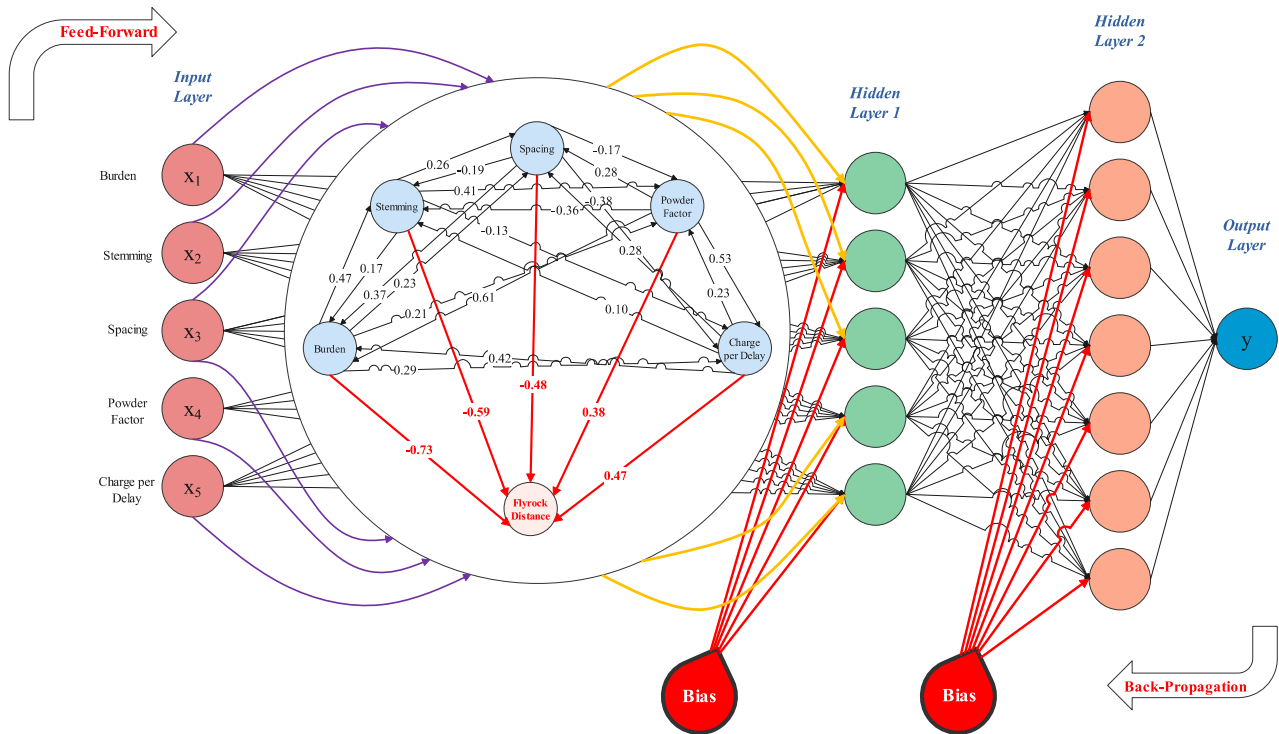
Fig. 9 Designing the ACWNNsR architecture with causal-and-effect relationships

Table 8 Performance indices for ACWNNsR models

Model	ACWNNsR architecture	Train			Test			Train rating			Test rating			Total rate	Total rank
		R^2	RMSE	VAF	R^2	RMSE	VAF	R^2	RMSE	VAF	R^2	RMSE	VAF		
ACWNNsR 1	5-3-1	0.935	3.511	92.353	0.848	6.315	85.362	2	4	1	1	2	1	11	10
ACWNNsR 2	5-5-1	0.926	5.049	92.925	0.923	6.180	92.163	1	1	2	3	3	3	13	8
ACWNNsR 3	5-7-1	0.980	2.752	98.277	0.975	3.722	97.660	5	6	5	6	6	6	34	7
ACWNNsR 4	5-10-1	0.955	3.871	95.803	0.981	3.210	98.195	4	3	4	8	9	8	36	6
ACWNNsR 5	5-3-5-1	0.988	2.350	99.121	0.969	4.147	96.977	9	8	9	4	5	4	39	4
ACWNNsR 6	5-5-7-1	0.996	1.404	99.867	0.991	2.535	99.136	10	10	10	10	10	10	60	1
ACWNNsR 7	5-7-9-1	0.988	2.191	99.075	0.970	4.370	97.028	8	9	8	5	4	5	39	4
ACWNNsR 8	5-8-10-1	0.981	2.920	98.448	0.983	3.308	98.398	6	5	6	9	8	9	43	2
ACWNNsR 9	5-9-12-1	0.983	2.627	98.591	0.978	3.422	97.904	7	7	7	7	7	7	42	3
ACWNNsR 10	5-10-13-1	0.954	3.875	95.699	0.875	6.610	87.661	3	2	3	2	1	2	13	8

Table 9 Performance indexes for the three developed models

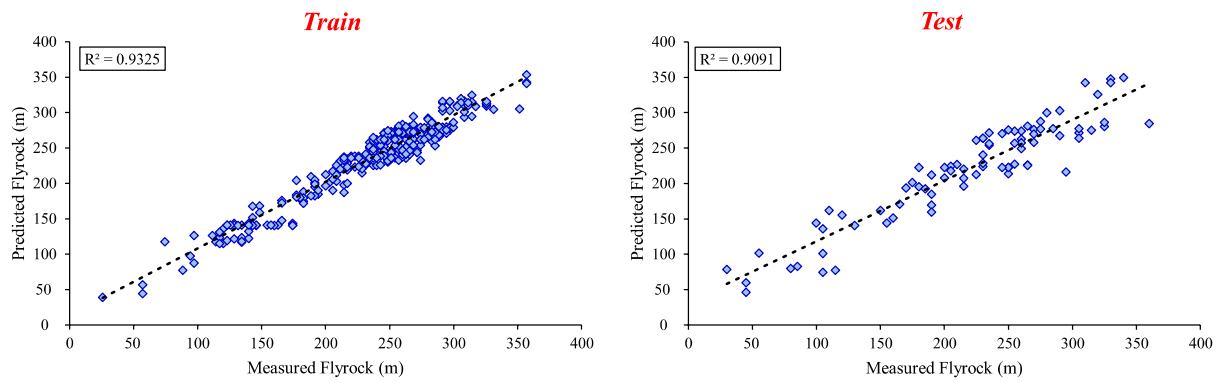| Model	Train			Test		
	R^2	RMSE	VAF	R^2	RMSE	VAF
MLP	0.932	5.000	93.849	0.909	6.618	92.188
BRNN	0.949	4.605	94.226	0.921	4.35	92.267
ACWNNsR	0.996	1.404	99.867	0.991	2.535	99.136

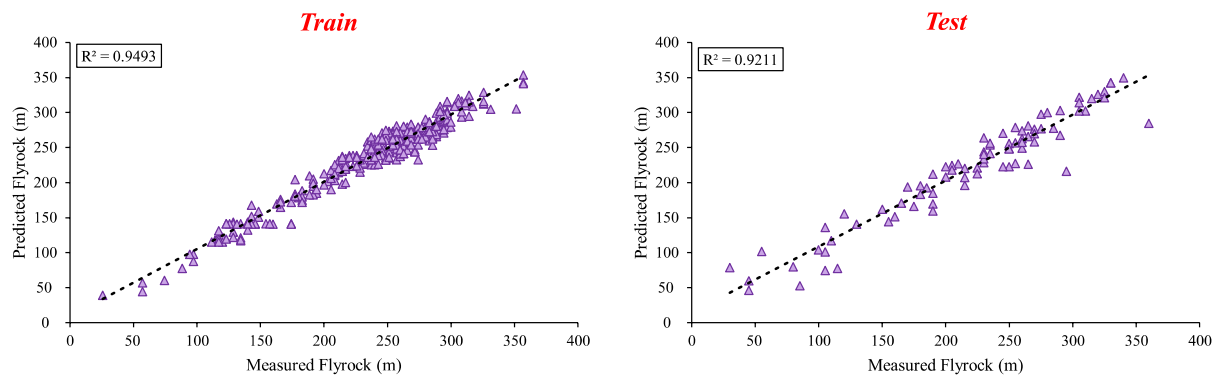**Fig. 10** Correlations of flyrock estimated by modeling MLP with actual values

Fig. 11 Correlations of flyrock estimated by modeling BRNN with actual values
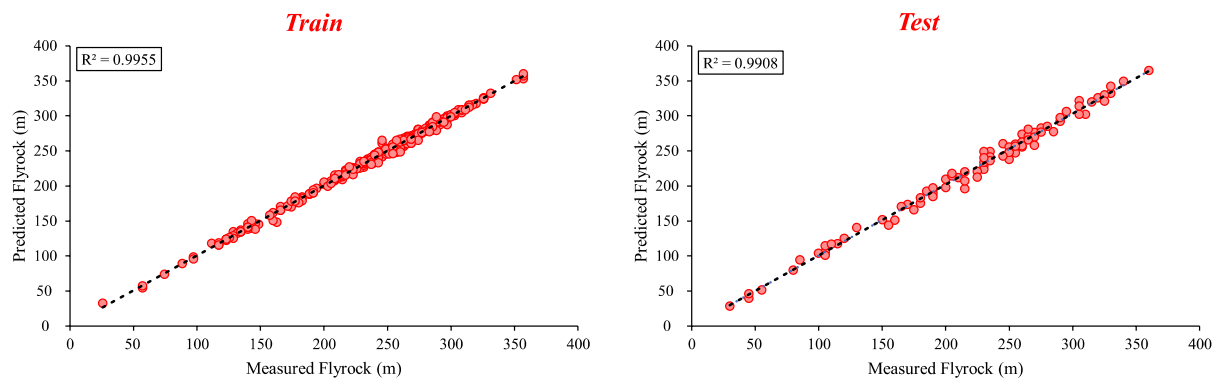

Fig. 12 Correlations of flyrock estimated by modeling ACWNNsR with actual values

spacing as the most influential parameter on flyrock distance, whereas the charge per delay indicates minor importance.

$$r_{ij} = \frac{\sum_{k=1}^{m} x_{ik} \cdot x_{jk}}{\sqrt{\left(\sum_{k=1}^{m} x_{ik}^2\right) \cdot \left(\sum_{k=1}^{m} x_{jk}^2\right)}} \tag{26}$$

$$E = \frac{\text{SSD}_i}{\sum_i \text{SSD}_i}, \quad \text{SSD}_i = \sum_p \left(\frac{\partial O_k^p}{\partial O_i^p}\right)^2. \tag{27}$$

In which y_{ik} and y_{jk} are the input and output parameters. m denotes the number of datasets, E is elements of data pairs participation of ith variable, O_k^p is output values for pattern

Fig. 13 Errors of flyrock prediction for testing datasets using MLP, BRNN, and ACWNNsR
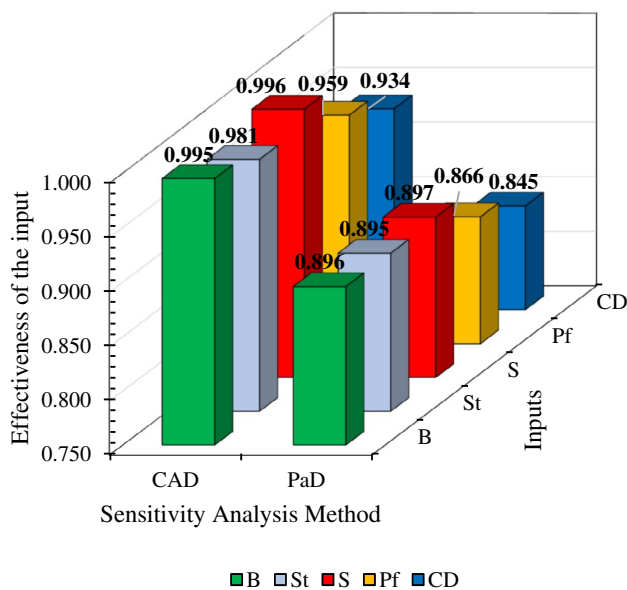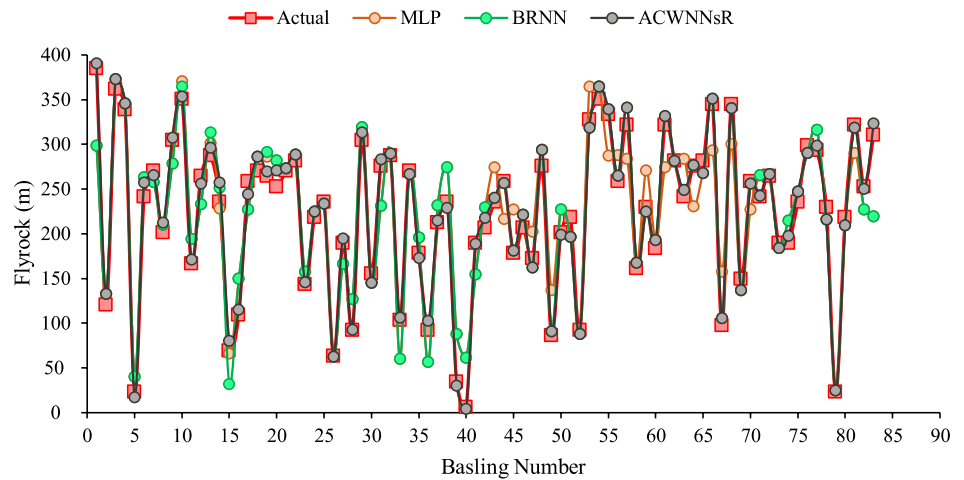

Fig. 14 The importance of effective parameters on flyrock distance

P, O_i^p indicates input values for pattern P, and SSD_i the sum of the squares of the partial derivatives. Notably, the highest E and r_{ij} value demonstrates the most influential inputs.

7 Conclusion

A new hybrid model based on the integration of multilayer perceptron neural networks (MLPNN) and fuzzy cognitive map (FCM) with the reliability of the Z-number concept was developed to predict flyrock distance induced by blasting operations. The developed model called artificial causality-weighted neural networks based on reliability (ACWNNsR) uses five effective, controllable parameters, including burden, stemming, spacing, powder factor, and charge per delay, to predict the flyrock distance. Performance indices of RMSE, VAF, and R^2 were determined to estimate the superiority of the predictive models. The ACWNNsR model resulted in R^2 of (0.996, 0.991), RMSE of (1.404, 2.535), and VAF of (99.867, 99.136) for train and test, respectively. The higher R^2 and VAF values and lower RMSE achieved by the ACWNNsR model than the conventional ANN and BRNN models show its success in providing a more accurate prediction flyrock distance. Notably, the proposed approach resulted in 62% and 42% improvement in the RMSE of the testing model in comparison to the MLP and BRNN models.

The effectiveness and relative significance of the effective parameters on flyrock distance was evaluated using a sensitivity analysis by Cosine Amplitude Method (CAM) and PaD method. The sensitivity analysis results showed the spacing has the most significant impact on flyrock distance, while charge per delay is the least important.

The presented approach is recommended for flyrock distance prediction in surface mines where buildings are close to the blasting site. Since the datasets used in this study were specific to the Anguran mine, applying the developed model in other projects would demand adjustments based on the employed blasting and mining operations. In addition, some limitations existed in the scope of this study that should be removed in future studies to increase the accuracy of the prediction. The applied dataset should be more comprehensive by including more controllable blasting parameters. The uncontrollable blasting parameters such as geomechanical properties of rock masses could also be monitored, measured, and involved for more accurate and reliable predictions.

Declarations

Conflict of interest The authors declare that they have no known competing financial interests or personal relationships that could have appeared to influence the work reported in this paper.

References

Abiyev RH, Uyar K, Ilhan U, Imanov E, Abiyeva E (2018) Estimation of food security risk level using *Z*-number-based fuzzy system. J Food Qual 2018:2760907

Aboutorab H, Saberi M, Asadabadi MR, Hussain O, Chang E (2018) ZBWM: the *Z*-number extension of best worst method and its application for supplier development. Expert Syst Appl. https://doi.org/10.1016/j.eswa.2018.04.015

Alizadeh S, Poormirzaee R, Nikrouz R, Sarmady S (2021) Using stacked generalization ensemble method to estimate shear wave velocity based on downhole seismic data: a case study of Sarab-E-Zahab, Iran. J Seism Explor 30:281–301

Armaghani DJ, Hajihassani M, Monjezi M, Mohamad ET, Marto A, Moghaddam MR (2015) Application of two intelligent systems in predicting environmental impacts of quarry blasting. Arab J Geosci 8(11):9647–9665

Armaghani DJ, Hasanipanah M, Mohamad ET (2016a) A combination of the ICA-ANN model to predict air-overpressure resulting from blasting. Eng Comput 32:155–171

Armaghani DJ, Mohamad ET, Hajihassani M, Abad SANK, Marto A, Moghaddam MR (2016b) Evaluation and prediction of flyrock resulting from blasting operations using empirical and computational methods. Eng Comput 32(1):109–121

Bakhtavar E, Hosseini S, Hewage K, Sadiq R (2021a) Green blasting policy: simultaneous forecast of vertical and horizontal distribution of dust emissions using artificial causality-weighted neural network. J Clean Prod 283:124562. https://doi.org/10.1016/j.jclepro.2020.124562

Bakhtavar E, Hosseini S, Hewage K, Sadiq R (2021b) Air pollution risk assessment using a hybrid fuzzy intelligent probability-based approach: mine blasting dust impacts. Nat Resour Res. https://doi.org/10.1007/s11053-020-09810-4

Esmaeili M, Osanloo M, Rashidinejad F, Bazzazi AA, Taji M (2014) Multiple regression, ANN and ANFIS models for prediction of backbreak in the open pit blasting. Eng Comput 30(4):549–558

Faradonbeh RS, Armaghani DJ, Monjezi M, Mohamad ET (2016) Genetic programming and gene expression programming for flyrock assessment due to mine blasting. Int J Rock Mech Min Sci 88:254–264

Fattahi H, Hasanipanah M (2021) An integrated approach of ANFIS-grasshopper optimization algorithm to approximate flyrock distance in mine blasting. Eng Comput 1:1–13

Gevrey M, Dimopoulos I, Lek S (2003) Review and comparison of methods to study the contribution of variables in artificial neural network models. Ecol Model 160:249–264

Ghasemi E, Amini H, Ataei M, Khalokakaei R (2012a) Application of artificial intelligence techniques for predicting the flyrock distance caused by blasting operation. Arab J Geosci 7:193–202. https://doi.org/10.1007/s12517-012-0703-6

Ghasemi E, Sari M, Ataei M (2012b) Development of an empirical model for predicting the effects of controllable blasting parameters on flyrock distance in surface mines. Int J Rock Mech Min Sci 52:163–170. https://doi.org/10.1016/j.ijrmms.2012.03.011

Ghoushchi SJ, Yousefi S, Khazaeili M (2019) An extended FMEA approach based on the Z-MOORA and fuzzy BWM for prioritization of failures. Appl Soft Comput 81:105505

Guo H, Nguyen H, Bui XN, Armaghani DJ (2021a) A new technique to predict fly-rock in bench blasting based on an ensemble of support vector regression and GLMNET. Eng Comput 37(1):421–435

Guo H, Zhou J, Koopialipoor M, Armaghani DJ, Tahir MM (2021b) Deep neural network and whale optimization algorithm to assess flyrock induced by blasting. Eng Comput 37(1):173–186

Hajihassani M, Armaghani DJ, Monjezi M, Mohamad ET, Marto A (2015) Blast-induced air and ground vibration prediction: a particle swarm optimization-based artificial neural network approach. Environ Earth Sci 74(4):2799–2817

Hasanipanah M, Amnieh HB (2020) A fuzzy rule-based approach to address uncertainty in risk assessment and prediction of blast-induced Flyrock in a quarry. Nat Resour Res 29(2):669–689

Hasanipanah M, Zhang W, Armaghani DJ, Rad HN (2020b) The potential application of a new intelligent based approach in predicting the tensile strength of rock. IEEE Access 8:57148–57157

Hasanipanah M, Keshtegar B, Thai DK, Troung NT (2020a) An ANN-adaptive dynamical harmony search algorithm to approximate the flyrock resulting from blasting. Eng Comput 38:1257–1269

Hosseini S, Monjezi M, Bakhtavar E, Mouasvi A (2021) Prediction of dust emission due to open pit mine blasting using a hybrid artificial neural network. Nat Resour Res. https://doi.org/10.1007/s11053-021-09930-5

Hosseini S, Poormirzaee R, Moosazadeh S (2022) Study of hazards in underground mining: using fuzzy cognitive map and *Z*-number theory for prioritizing of effective factors on occupational hazards in underground mines. Iran J Min Eng (**In press**)

Jiskani IM, Yasli F, Hosseini S, Rehman AU, Uddin S (2022) Improved *Z*-number based fuzzy fault tree approach to analyze health and safety risks in surface mines. Resour Policy 76:102591. https://doi.org/10.1016/j.resourpol.2022.102591

Jong YH, Lee CI (2004) Influence of geological conditions on the powder factor for tunnel blasting. Int J Rock Mech Min Sci. https://doi.org/10.1016/j.ijrmms.2004.03.095

Kalaivaani PT, Akila T, Tahir MM, Ahmed M, Surendar A (2020) A novel intelligent approach to simulate the blast-induced flyrock based on RFNN combined with PSO. Eng Comput 36:435–442

Keshtegar B, Hasanipanah M, Nguyen-Thoi T, Yagiz S, Bakhshandeh AH (2021) Potential efficacy and application of a new statistical meta based-model to predict TBM performance. Int J Min Reclam Environ 7:471–487

Khandelwal M, Monjezi M (2013a) Prediction of backbreak in open-pit blasting operations using the machine learning method. Rock Mech Rock Eng 46(2):389–396

Khandelwal M, Monjezi M (2013b) Prediction of flyrock in open pit blasting operation using machine learning method. Int J Min Sci Technol. https://doi.org/10.1016/j.ijmst.2013.05.005

Kurnaz TF, Kaya Y (2018) The comparison of the performance of ELM, BRNN, and SVM methods for the prediction of compression index of clays. Arab J Geosci 11(24):1–14

Lu X, Hasanipanah M, Brindhadevi K, Amnieh HB, Khalafi S (2020) ORELM: a novel machine learning approach for prediction of flyrock in mine blasting. Nat Resour Res 29(2):641–654

Lundborg N, Persson A, Ladegaard-Pedersen A, Holmberg R (1975) Keeping the lid on flyrock in open-pit blasting. Eng Min J 176:95–100

Mackay DJC (1992) Bayesian methods for adaptive models. Ph.D. thesis, California Institute of Technology

Marto A, Hajihassani M, Jahed AD, Tonnizam ME, Makhtar AM (2014) A novel approach for blast-induced flyrock prediction based on imperialist competitive algorithm and artificial neural network. Sci World J 5:643715

McCulloch WS, Pitts W (1943) A logical calculus of the ideas immanent in nervous activity. Bull Math Biophys 5:115e133

McKenzie CK (2009) Flyrock range and fragment size prediction. In: Proceedings of the 35th annual conference on explosives and blasting technique, 2. International Society of Explosives Engineers

Monjezi M, Khoshalan HA, Varjani AY (2012) Prediction of flyrock and backbreak in open pit blasting operation: a neuro-genetic approach. Arab J Geosci 5:441–448

Murlidhar BR, Kumar D, Armaghani DJ, Mohamad ET, Roy B, Pham BT (2020) A novel intelligent ELM-BBO technique for predicting distance of mine blasting-induced flyrock. Nat Resour Res 29(6):4103–4120

Nguyen H, Bui X-N (2020) Soft computing models for predicting blast-induced air over-pressure: a novel artificial intelligence approach. Appl Soft Comput 92:106292

Nguyen H, Bui X-N, Bui H-B, Mai N-L (2020) A comparative study of artificial neural networks in predicting blast-induced air-blast overpressure at Deo Nai open-pit coal mine. Vietnam Neural Comput Appl 32:3939–3955

Onari MA, Yousefi S, Rezaee MJ (2020) Risk assessment in discrete production processes considering uncertainty and reliability: Z-number multi-stage fuzzy cognitive map with fuzzy learning algorithm. Artif Intell Rev 54:1349–1383

Papageorgiou EI, Kannappan A (2012) Fuzzy cognitive map ensemble learning paradigm to solve classification problems: application to autism identification. Appl Soft Comput 12:3798–3809

Poormirzaee R, Hosseini S (2021) Selection of surface mines reclamation strategies based on renewable energies using a new hybrid method. J Miner Resour Eng. https://dx.doi.org/10.30479/jmre.2021.15678.1520

Rad HN, Hasanipanah M, Rezaei M, Eghlim AL (2018) Developing a least squares support vector machine for estimating the blast-induced flyrock. Eng Comput 34:709–717

Rad HN, Bakhshayeshi I, Jusoh WAW, Tahir MM, Foong LK (2020) Prediction of flyrock in mine blasting: a new computational intelligence approach. Nat Resour Res 29:609–623

Raina AK, Chakraborty AK, Ramulu M, Sahu PB, Haldar A, Choudhury PB (2004) Flyrock prediction and control in opencast mines: a critical appraisal. Min Eng J 6(5):10–20

Rezaee MJ, Yousefi S, Babaei M (2017) Multi-stage cognitive map for failures assessment of production processes: an extension in structure and algorithm. Neurocomputing. https://doi.org/10.1016/j.neucom.2016.10.069

Rezaee MJ, Yousefi S, Hayati J (2018) A decision system using fuzzy cognitive map and multi-group data envelopment analysis to estimate hospitals' outputs level. Neural Comput Appl 29:761–777

Rezaee MJ, Yousefi S, Baghery M, Chakrabortty RK (2021) An intelligent strategy map to evaluate improvement projects of auto industry using fuzzy cognitive map and fuzzy slack-based efficiency model. Comput Ind Eng 151:106920

Sari M, Ghasemi E, Ataei M (2014) Stochastic modeling approach for the evaluation of backbreak due to blasting operations in open pit mines. Rock Mech Rock Eng 47(2):771–783

Shahin MA, Maier HR, Jaksa MB (2002) Predicting settlement of shallow foundations using neural networks. J Geotech Geoenviron Eng 128:785–793

Simpson PK (1990) Artificial neural system: foundation, paradigms, applications and implementations. Pergamon, New York

Siskind DE, Kopp JW (1995) Blasting accidents in mines, a 16-year summary. International Society of Explosives Engineers, Cleveland

Song C, Wang J-Q, Li J-B (2020) New framework for quality function deployment using linguistic Z-numbers. Mathematics 8:224

Taheri K, Hasanipanah M, Golzar SB, Abd Majid MZ (2017) A hybrid artificial bee colony algorithm-artificial neural network for forecasting the blast-produced ground vibration. Eng Comput 33:689–700

Tian Y, Mi X, Cui H, Zhang P, Kang B (2021) Using Z-number to measure the reliability of new information fusion method and its application in pattern recognition. Appl Soft Comput 111:107658

Trivedi R, Singh TN, Gupta N (2015) Prediction of blast-induced flyrock in opencast mines using ANN and ANFIS. Geotech Geol Eng 33:875–891

Yaakob AM, Gegov A (2016) Interactive TOPSIS based group decision making methodology using Z-numbers. Int J Comput Intell Syst 9:311–324

Yari M, Bagherpour R, Jamali S, Shamsi R (2016) Development of a novel flyrock distance prediction model using BPNN for providing blasting operation safety. Neural Comput Appl 27:699–706

Yazdi M, Hafezi P, Abbassi R (2019) A methodology for enhancing the reliability of expert system applications in probabilistic risk assessment. J Loss Prev Process Ind 58:51–59

Zadeh LA (2011) A note on Z-numbers. Inf Sci 181(14):2923–2932

Zhou J, Li C, Koopialipoor M, Jahed AD, Thai PB (2020) Development of a new methodology for estimating the amount of PPV in surface mines based on prediction and probabilistic models (GEP-MC). Int J Min Reclam Environ 35:48–68

Zorlu K, Gokceoglu C, Ocakoglu F, Nefeslioglu HA, Acikalin S (2008) Prediction of uniaxial compressive strength of sandstones using petrography-based models. Eng Geol 96:141–158